Design and Hardware-In-the-Loop Validation of an IEC 61850-Based Coordinated Protection Scheme for Large-Scale Wind Farm Integration in Smart Grids

Y. Gcelu[1*], M.E.S. Mnguni[2], S. Nomandela[3*]
[1,2]Department of Electrical, Electronic and Computer Engineering, Faculty of Engineering and the Built Environment, Cape Peninsula University of Technology, Bellville, P.O. Box 1906, Cape Town 7353, South Africa
[3]Department of Electrical Engineering, Faculty of Engineering, Built Environment and Information Technology, iYunivesithi Walter Sisulu, Buffalo City Campus, College Street, East London 5200, South Africa
[*]corresponding authors' emails: yongamagcelu@gmail.com, snomandela@wsu.ac.za

Abstract – *This paper presents the design, implementation, and validation of a coordinated protection scheme for high-voltage (HV) transformers integrated with a large-scale wind farm (LSWF) within a smart-grid environment. The proposed system is based on the IEC 61850 communication standard, employing Generic Object-Oriented Substation Event (GOOSE) messaging to achieve high-speed coordination among Intelligent Electronic Devices (IEDs). A modified IEEE 9-bus power system integrated with eighteen Vestas V117-4.2 MW wind turbine generator units (WTGUs) was modeled on the Real-Time Digital Simulator (RTDS) using RSCAD FX. The primary protection is implemented with the SEL-487E differential relay, while backup protection is provided by the SEL-751A feeder IED. Hardware-in-the-loop (HIL) validation using the Omicron CMC 356 verified both the fault-detection speed and GOOSE communication latency under internal and external fault scenarios. Results show that the proposed IEC 61850-based protection scheme enhances fault detection accuracy, coordination reliability, and response speed compared to conventional methods.*

Keywords: *Hardware-in-the-loop, IEC 61850, large-scale wind farm, smart grid, transformer differential protection*

Article History
Received 16 April 2026
Received in revised form 25 June 2026
Accepted 16 July 2026

I. Introduction

The global transition toward smart and sustainable energy systems has accelerated the integration of renewable power plants (RPPs) into electrical grids [1]–[2]. Wind energy has grown rapidly owing to its environmental benefits and declining levelized cost of electricity. Consequently, many large-scale wind farms (LSWFs) now operate at the transmission level and are interconnected with existing utility grids [3]–[4]. This interconnection introduces complex transients and reduced fault currents, challenging conventional protection schemes [5]–[6].

Protection reliability is critical at the interface between LSWFs and the main grid, where high-voltage (HV) transformers form the point of common coupling (PCC). These costly and sensitive transformers require fast, selective, and dependable protection [7]–[8], achieved through coordinated differential and backup elements that adapt to variable wind conditions.

The IEC 61850 standard addresses these challenges by enabling standardized, high-speed, and interoperable substation communication [9]. Its Generic Object-Oriented Substation Event (GOOSE) service allows peer-to-peer signaling within milliseconds, while the Manufacturing Message Specification (MMS) supports supervisory communication [10]. Coupled with hardware-in-the-loop (HIL) validation, IEC 61850 enables digital protection systems that closely replicate real substation behavior [11]–[12]. However, few studies have demonstrated IEC 61850-based coordination for HV transformer protection in wind-integrated smart grids, with most research limited to simulation or medium voltage (MV) applications [13]–[16]. The influence of communication latency and GOOSE reliability on trip coordination also remains insufficiently quantified.

Recent studies published between 2024 and 2026 further confirm the growing importance of IEC 61850-based communication, digital substations, programmable digital twins, GOOSE-based event transfer, and

This is an Open Access article distributed under the terms of the Creative Commons Attribution-Noncommercial 3.0 Unported License, permitting copy and redistribution of the material and adaptation for commercial and uncommercial use.

interoperability between protection and automation devices [17]–[21]. In addition, recent HIL-based protection and monitoring platforms show that real-time validation is becoming essential for verifying the behavior of IEC 61850-based schemes under realistic operating conditions before field deployment [22]. These developments support the need for practical validation of communication-assisted protection schemes rather than relying only on offline simulations.

Smart grids combine traditional power networks with information and communication technologies to enhance reliability and efficiency [1]–[2]. Intelligent Electronic Devices (IEDs) within generation, transmission, and distribution zones provide real-time monitoring and protection [7]. Bidirectional power flow from distributed generation requires multilayered protection capable of isolating faults quickly and selectively [8], ensuring security and dependability under dynamic conditions [9].

Wind farms equipped with doubly-fed induction generators (DFIGs) produce limited, variable fault currents that compromise overcurrent-based protection [3], [10]. Moreover, low-voltage ride-through (LVRT) requirements improve stability but complicate relay coordination [11]–[13].

Effective protection in wind-integrated grids must detect and isolate internal transformer faults rapidly and securely, adapt to fluctuating wind conditions, and coordinate across voltage levels [14]. Traditional impedance protection often proves inadequate due to harmonic distortion and inconsistent fault impedance from DFIGs [7]. Hence, hybrid and adaptive schemes have been proposed to maintain selectivity and sensitivity [16].

The increasing penetration of inverter-based renewable energy resources has further intensified protection challenges in smart grids and wind-integrated networks. Recent studies indicate that converter-dominated networks can alter the magnitude, direction, and frequency of fault currents, thereby affecting the performance of distance, differential, and overcurrent protection [23]–[26]. Other recent contributions have proposed adaptive, active-power-based, data-driven, and differential fault-detection methods to improve sensitivity and selectivity under changing operating conditions [27]–[29]. For wind-farm transmission systems, protection methods based on high-frequency impedance and other signal features have also been proposed to address the changing fault behavior of renewable-based generation [30].

IEC 61850 defines a global framework for substation automation, featuring Logical Nodes (LNs), Substation Configuration Language (SCL), and communication models such as GOOSE, MMS, and Sampled Values (SV). GOOSE messaging supports sub-4 ms latency for peer-to-peer event exchange, while MMS and SV handle supervisory and time-synchronized measurements. Prior studies confirm that IEC 61850 reduces wiring complexity and enhances coordination [31]–[32], but implementations for HV transformers in wind farms remain limited [33].

Research continues to highlight reliability and coordination challenges in renewable-integrated smart grids [3], [4], [34]. DFIG-based wind farms exhibit low and inconsistent fault currents, which can lead to potential relay miscoordination [2], [3]. Adaptive impedance and frequency-based schemes have been proposed to mitigate these effects [12], [16], while dual-slope differential and real-time IEC 61850 coordination approaches have shown promise [5], [31], [35]. Despite progress, full-scale HV validation using real-time HIL remains scarce [32], [33].

Recent review studies also emphasize that future smart-grid and microgrid protection must be adaptive, communication-assisted, and capable of coordinating multiple protection layers under bidirectional power flow and variable fault-current conditions [36]–[39]. These findings reinforce the motivation of the present study, particularly the need for coordinated differential–overcurrent protection that combines IEC 61850 GOOSE messaging, real IED operation, and HIL validation in a renewable-energy-integrated smart-grid environment.

Three research gaps persist: (1) lack of integrated multilayer schemes coordinating main and backup protection across voltage levels [34]; (2) limited IEC 61850 application in HV transformer zones [31]; and (3) insufficient real-time validation of coordinated IEDs via RTDS and Omicron platforms [32]. IEC 61850 and HIL testing are recognized as key enablers of next-generation smart-grid protection, yet practical verification in LSWF transformer protection is limited.

This paper presents the design and HIL validation of an IEC 61850-based coordinated protection scheme for HV transformers integrated with an LSWF. The configuration employs an SEL-487E Differential Protection Relay as the main protection and an SEL-751A Feeder Protection Relay as the backup. For consistency, the SEL-487E Differential Protection Relay and SEL-751A Feeder Protection Relay are hereafter referred to as the SEL-487E relay and SEL-751A relay, respectively. Both relays communicate via GOOSE messaging over an Ethernet-based substation network modeled in RTDS/RSCAD FX. Experimental verification using an Omicron CMC 356 test set confirms that the proposed scheme improves fault-clearing speed, coordination accuracy, and overall reliability in wind-integrated smart grids.

The remainder of this paper is organized as follows: Section II describes the modeling and simulation of the smart-grid system and base-case conditions; Section III presents the design and integration of the IEC 61850-based protection scheme; Section IV discusses the simulation and testing results; and Section V provides conclusions and recommendations for future work.

II. Smart Grid System Considered for the Study

A. Modeling and Modifications

The proposed protection scheme was implemented on a large-scale wind-integrated smart grid system modeled in RSCAD FX and executed on the RTDS platform. The network was derived from the IEEE 9-bus test system, modified to include a 75.6 MW LSWF comprising 18 Vestas V117-4.2 MW WTGUs. These units were arranged into three collector feeders, each comprising six WTGUs connected to a 24 kV collector bus, which in turn was interfaced with a 24 kV/230 kV step-up transformer representing the PCC with the main grid.

To achieve real-time performance, the smart-grid model was distributed across five RTDS PB5 racks: two racks simulated the IEEE 9-bus subsystem, while three racks hosted the wind-farm groups. The load-flow base power was 100 MVA, and the voltage profile was maintained between 0.98 and 1.02 p.u. under steady-state conditions. The model enabled the simulation of symmetrical and asymmetrical fault scenarios, thereby facilitating differential and overcurrent relay coordination studies. Fig. 1 presents the single-line diagram of the implemented network.

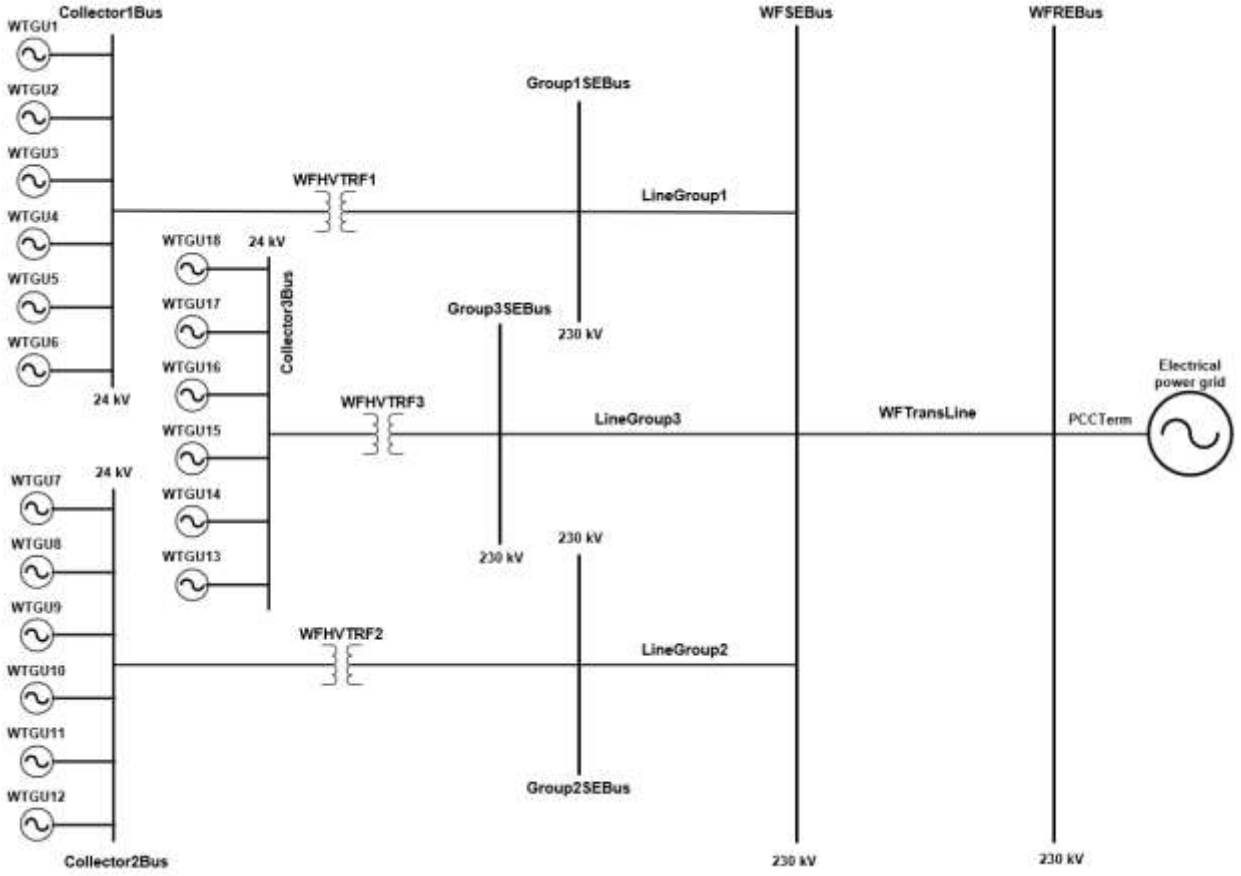


Fig. 1. Single-phase representation of the resultant smart grid system [40]

TABLE I
SPECIFICATIONS ADOPTED FOR THE SIMULATED INVERTER

ABBREVIATION	MEANING
WTGU	Wind turbine generator unit
WFHVTRF1	Wind farm high-voltage transformer
WFSEBus	Wind farm sending-end busbar
WFREBus	Wind farm receiving-end busbar
	Wind farm transmission line (possible grid connection point)

The component labeled “electrical power grid” in the smart grid system in Fig. 1 represents the IEEE 9-bus power system. Nonetheless, the simulations conducted in this study, under the increased load-demand condition, verified that the busbar voltages remained stable.

The system above, originally studied in [40], was modeled to operate under two conditions: initial and increased load demand conditions. However, this study considers only the condition of increased load demand and

treats that as the base simulations. This is to say that the simulations presented in Section II.B below are based on the increased-load demand simulations but are merely base simulations for this study.

B. Fundamental Simulations

The simulations of the smart grid system in this section were done under conditions and assumptions listed in Tables II and III. Table II summarizes the environmental and operational assumptions adopted for the large-scale wind farm side, while Table III summarizes the loading and generation assumptions adopted for the IEEE 9-bus system side.

TABLE II
CONDITIONS AND ASSUMPTIONS ON THE LARGE-SCALE WIND FARM SIDE

PARAMETER	VALUE	REASON/JUSTIFICATION WHERE APPLICABLE
Temperature (°C)	25	The wind turbines in this smart grid system operate within a temperature range of −20 °C to 45 °C. When the temperature remains within this range, the turbines can be tuned to deliver a power output close to their rated capacity.
Humidity (%)	30	—
Air pressure (mbar)	1415	—
Wind speed (m/s)	14	WTs are expected to generate the rated output power at this speed.
Pitch angle (°)	32	—
Number of wind turbine generator units (WTGUs) operating at the same time	18 (all)	All WTGUs were assumed to operate simultaneously in the base-case simulation.

It is important to note that not all WTGUs in a wind farm operate simultaneously. Their operation typically depends on the load demand, which is managed through control methods that determine which units should run at any given time. However, no control system was implemented to regulate the number of operating WTGUs in the original study, which adopted the smart grid system. Additionally, the load demand was modeled based on a worst-case scenario.

TABLE III
CONDITIONS AND ASSUMPTIONS ON THE IEEE 9-BUS SYSTEM SIDE

SYSTEM PARAMETER	COMPONENT/ LOAD	VALUE/STATEMENT
Load demand (MVA)	DLoad1	172.5
Load demand (MVA)	DLoad2	131.9
Load demand (MVA)	DLoad3	143.1
Number of traditional generators operating at a time	Synchronous generators	3 (all)
System parameter	Component/Load	Value/Statement

Using the conditions listed in Tables II and III, the load flow simulation on steady-state conditions of the smart grid system was performed in this study to check if the busbar voltages were in the acceptable range of 0.95 to 1.05 p.u for traditional electrical power grids and 0.9 to 1.0985 p.u for LSWFs as per the grid code specifications. Table IV shows the apparent power on loads and corresponding busbar voltages.

TABLE IV
SPECIFICATIONS ADOPTED FOR THE SIMULATED INVERTER. APPARENT POWER ON LOADS AND BUSBAR VOLTAGES IN THE STEADY-STATE SIMULATION OF THE SMART GRID SYSTEM

LOADS/BUSBAR	LOAD APPARENT POWER (MVA)	BUSBAR VOLTAGE (PU)
Bus1	—	0.9981
DLoad1|Bus2	172.5	0.9558
DLoad2|Bus3	131.9	0.9707
Bus4	—	0.9975
DLoad3|Bus5	143.1	0.9801
Bus6	—	1.004
Coll1Bus	—	0.9458
Coll2Bus	—	0.9458
Coll3Bus	—	0.9458
WF1SEBus	—	0.9548
WF1REBus	—	0.9561

The value of the voltages recorded in Table IV is satisfactory in terms of being within the specified ranges.

Developing a differential protection scheme for a power transformer requires knowledge of the steady-state currents flowing through it.

These currents are used to select instrument transformers and set threshold values for differential protection relay elements. While the steady-state simulations of the smart grid system were performed, currents through the power transformers connecting the LSWF to the electrical power grid were also monitored, as recorded in Table V.

TABLE V
CURRENTS RECORDED FROM THE PRIMARY AND SECONDARY SIDES OF THE MV TO HV STEP-UP TRANSFORMERS FOR EACH WIND TURBINE GENERATOR UNIT

LARGE-SCALE WIND FARM SIDE HIGH-VOLTAGE STEP-UP POWER TRANSFORMERS	MEDIUM-VOLTAGE SIDE CURRENTS (KA)	HIGH-VOLTAGE SIDE CURRENTS (KA)
Group1Trans	0.5942	0.0623
Group2Trans	0.5942	0.0623
Group3Trans	0.5942	0.0623

However, it should be noted that the protection scheme will be tested only in the transformer group, Group1Trans.

The fundamental simulations performed above were designed to validate the accuracy of the data at steady-state conditions. During the simulations, the voltages and currents were monitored and recorded. As part of the

requirements stated in the book Electric Power Systems [41], such as ensuring that the busbar voltages are within the acceptable operating ranges for electrical power systems before using them for various studies, and that the voltage results obtained from the interconnected system studied above are satisfactory. The currents simulated and recorded in Table V were used in the next sections to develop the proposed protection scheme.

III. Design and Integration of IEC 61850-based Protection Scheme

A. Overview of the Proposed Protection Scheme

The proposed protection scheme focuses on the HV step-up transformer, where different fault conditions may occur within or near the protected zone. The scheme integrates primary and backup protection layers to ensure fast, selective, and dependable fault isolation while reducing the risk of maloperation or missed tripping.

The primary protection function is provided by transformer differential protection, which detects internal faults within the protected transformer zone. The backup protection function is provided by overcurrent protection, which operates when the primary protection fails to detect or clear a fault. This layered arrangement improves the dependability and security of the overall protection system.

The SEL-487E relay is used as the primary protection relay. It is configured with restrained and unrestrained differential elements, slope-based differential thresholds, operating and restraint characteristics, and harmonic blocking to improve security during conditions such as CT saturation and magnetizing inrush. The SEL-751A relay is configured as the backup relay and provides time-coordinated overcurrent protection when the SEL-487E does not issue a successful trip.

In the RSCAD FX model, the Giga-Transceiver Analog Output (GTAO) cards are assigned to the CT signals used by the physical IEDs. Therefore, selecting appropriate CT ratios and related instrument-transformer parameters is required before configuring the GTAO channels. This ensures that the analog signals supplied from the real-time simulation to the protection relays accurately represent the transformer currents under normal and faulted operating conditions.

B. Current Transformer Selection on RSCAD FX

The full-load currents, derived from a transformer rated at 30 MVA with voltage levels of 24 kV/230 kV, were 0.7217 kA on the primary (MV) side and 0.0753 kA on the secondary (HV) side. These values were used to determine the appropriate CT ratings. In line with the IEEE Guide for Selecting Protection Current Transformers [42], the recommended primary CT current ratio should range from 120% to 150% of the full-load current.

Accordingly, the CT ratios were set at 150% to establish the medium-voltage current transformer ratio (MVCTCR) and the high-voltage current transformer ratio (HVCTCR).

The current ratio of the MV side CTs for both SEL-487E and SEL-751A relays:

$$\mathrm{MVCT_{CR}} = 150\% \times \mathrm{I_{MV}} \tag{1}$$

$$\mathrm{MVCT_{CR}} = 150\% \times 0.7217\ \mathrm{kA}$$

$$\mathrm{MVCT_{CR}} = 1082.55\ \mathrm{A}$$

The current ratio of the HV side CT for the SEL-487E relay:

$$\mathrm{HVCT_{CR}} = 150\% \times \mathrm{I_{HV}} \tag{2}$$

$$\mathrm{HVCT_{CR}} = 150\% \times 0.0753\ \mathrm{kA}$$

$$\mathrm{HVCT_{CR}} = 112.9599\ \mathrm{A}$$

Based on the IEEE guide for CT selection, the closest ratios were selected, resulting in 1200:5 for $\mathrm{MVCT_{CR}}$ (primary side) for SEL-487E and SEL-751A, and 200:5 for $\mathrm{HVCT_{CR}}$ (secondary side) for SEL-487E, respectively.

The names of the CTs are CT0 for SEL-751A, CT1 for the MV side of the SEL-487E, and CT2 for the HV side of the SEL-487E.

C. Configuration of the SEL-487E Station Phasor Measurement Unit

The SEL-487E relay serves as the primary protection device, employing both restrained and unrestrained differential protection elements. This section outlines how the relay settings were configured based on calculated thresholds and how these configurations were implemented using the AcSELerator QuickSet software.

Restrained differential pickup settings (O87P). The restrained differential pickup threshold, denoted as O87P, was determined using the following formula:

$$\mathrm{O87P} \geq 10\% \left(\frac{\mathrm{I_{Nominal}}}{\mathrm{TAPS}}\right) \tag{3}$$

Assuming a nominal current $\mathrm{I_{Nominal}}$ = 1 A and TAPS = 3.01 A (tap value for selected CT secondary):

$$\mathrm{O87P} \geq 10\% \left(\frac{1\ \mathrm{A}}{3.01\ \mathrm{A}}\right)$$

$$\mathrm{O87P} \geq 0.0332$$

This setting ensures that the relay only operates for faults exceeding 3.32% of the selected tap input, thereby avoiding nuisance tripping.

Unrestrained differential pickup settings (U87P). The unrestrained pickup threshold U87P is configured as follows:

$$\mathrm{U87P} = 167\% \left(\frac{\mathrm{I_{FullLoad}} \left(\frac{\mathrm{I_{SecR}}}{\mathrm{I_{PrimR}}} \right)}{\mathrm{TAPS}} \right) \quad (4)$$

Where $I_{Nomal\ Load}$ = 0.7217 kA, I_{SecR} = 5 A, I_{PrimR} = 1200 A, and TAPS = 3.01 A.

$$\mathrm{U87P} = 167\% \left(\frac{0.7217\ \mathrm{kA} \left(\frac{5}{1\,200} \right)}{3.01\ \mathrm{A}} \right)$$

$$\mathrm{U87P} = 0.999$$

The above calculations were done based on the MV side of the protected transformer Group1Trans. They ensure that during severe internal faults, the relay responds instantly without requiring restraint calculation.

The SEL-487E relay was then configured using AcSELerator QuickSet software, specifying the CT values, differential elements, slope settings, and output trip equations to trip the circuit breaker.

These configurations collectively ensure the secure and dependable operation of the SEL-487E relay under various system conditions.

D. Configuration of the SEL-751A Feeder Protection Relay

The SEL-751A IED was also configured to operate as a backup protection device, primarily using time-overcurrent (51P1P) elements.

Overcurrent pickup setting (51P1P). The pickup current setting I_{Set} was calculated using the measured load current on the MV side of the protected transformer Group1Trans, which was 0.5942 kA. The relay uses a nominal current I_{Nom} = 5 A, and the CT ratio is 1200:5.

The overcurrent pickup percentage (PS) is calculated as follows:

$$\left(\frac{\mathrm{I_{Prime}}}{\mathrm{CT_{PTurns}}} \right) = (90\%)(\mathrm{I_{Set}}) = (90\%)(\mathrm{PS})(\mathrm{I_{Nom}})$$

$$\mathrm{PS} = \frac{\mathrm{I_{Prime}} \left(\frac{\mathrm{I_{SecR}}}{\mathrm{I_{PrimeR}}} \right)}{(90\%)(\mathrm{I_{Nom}})}$$

$$\mathrm{PS} = \frac{0.5942\ \mathrm{kA} \left(\frac{5\ \mathrm{A}}{1\,200\ \mathrm{A}} \right)}{(90\%)(5\ \mathrm{A})}$$

$$\mathrm{PS} = 55.0185\%$$

From this percentage, the pickup current is:

$$\mathrm{I_{Set}} = \mathrm{I_{51P1P}} = 55.0185\% \times 5\ \mathrm{A}$$

$$\mathrm{I_{51P1P}} = 2.7509\ \mathrm{A}$$

However, due to software constraints in the pickup settings block (which limits the input range to 0.10 A to 3.20 A), a rounded-down value of 2.5 A was selected for setting 51P1P.

Time delay setting. The time delay for this overcurrent element was configured with a standard inverse-time characteristic and a time multiplier setting (TMS) of 1. This delay ensures coordination with the SEL-487E relay, allowing primary protection a chance to clear faults before backup operation.

Torque control and logic implementation. To coordinate with the SEL-487E and prevent redundant tripping, GOOSE-based torque blocking was implemented using virtual bits VB001 (87R) and VB002 (87U). When either bit is received, the torque control logic blocks the overcurrent element.

The logic also includes Pushbutton 1 (PB01) and Pushbutton 2 (PB02). These are manual pushbuttons for latch and block control. Target LED 6 (T06_LED) is a visual indicator on the front panel that lights up upon receipt of a GOOSE message, confirming torque blocking activation.

SEL-751A Relay setup in AcSELerator QuickSet. The SEL-751A relay was also configured, specifying the CT values, overcurrent pickup setting, and trip logic, which was mapped to the output contacts of the relay for circuit breaker (CB) tripping.

These settings ensure that the SEL-751A operates reliably as a backup device and only trips when the SEL-487E either fails to detect or is unable to act on a fault.

Time delay setting. The time delay for this overcurrent element was configured with a standard inverse-time characteristic and a TMS of 1. This delay ensures coordination with the SEL-487E relay, allowing primary protection a chance to clear faults before backup operation. The final SEL-751A backup relay settings adopted for the time-overcurrent element are summarized in Table VI.

TABLE VI
SEL-751A RELAY SETTINGS

PROTECTION ELEMENT	DESCRIPTION	SETTING CURRENT (A)	TIME DIAL/TMS	CHARACTERISTIC
51P1P	Level 1 maximum phase time-overcurrent element pickup	2.5	1	$\text{TMS}\left(\frac{0.14}{(\text{M})^{0.02}-1}\right)$

E. Hardware-In-the-Loop Simulation Test Setup on RSCAD FX

This setup used the RTDS to generate analog signals representing CT outputs, transmitted to the SEL-487E and SEL-751A via GTAO modules. CT0, CT1, and CT2 were configured to match the selected CT parameters, e.g., 180:1 turns ratio, and series resistances. Proper burden resistance and scaling ensured accurate, phase-coherent analog inputs for precise differential and restraint current calculations.

The CT labels, primary current signal names, secondary series resistance values, turns ratios, and secondary current signal names used in the RSCAD FX HIL setup are summarized in Table VII.

All CTs were assigned to dedicated GTAO channels, as shown in Fig. 2. These modules interface the RTDS with the physical SEL-487E and SEL-751A IEDs by converting simulated current signals into ±10 V DC analog voltages. Each channel was calibrated to match the full-load current levels of the transformer, scaled to fit the 5 A nominal secondary input of the relay based on the CT ratios, e.g., 1200:5 for the MV side and 200:5 for the HV side.

The GTAO outputs were verified in real time using RSCAD meters to confirm waveform integrity, phase alignment, and amplitude fidelity. These checks ensured that the injected currents accurately reflected the simulated electrical behavior of the system under both normal and faulted conditions.

TABLE VII
CT SETTING VALUES

CT LABEL	PRIMARY CURRENT SIGNAL NAMES: PHASES R, Y, B	SECONDARY SERIES RESISTANCE (Ω)	TURNS RATIO	SECONDARY CURRENT SIGNAL NAMES: PHASES R, Y, B
CT0	Group1BRKIR	0.61	240	CT0ISec
	Group1BRKIY			CT0ISecY
	Group1BRKIB			CT0ISecB
CT1	Group1TransIPrIR	0.61	240	CT1ISecR
	Group1TransIPrIY			CT1ISecY
	Group1TransIPrIB			CT1ISecB
CT2	Group1TransISecIR	0.10	40	CT2ISecR
	Group1TransISecIY			CT2ISecY
	Group1TransISecIB			CT2ISecB

CT configurations followed IEEE Std C57.13 guidelines for selection and saturation avoidance, ensuring dependable differential protection. Accurate current replication enabled the SEL-487E relay to compute differential and restraint currents correctly for 87R and 87U tripping.

The analog simulation and relay behavior formed a closed-loop protection system in which simulated faults produced analog current injections into the SEL-487E and SEL-751A relays. Upon detecting a fault, a relay issued a trip signal to operate a virtual CB in RTDS/RSCAD FX via the Giga-Transceiver Front Panel Interface (GTFPI) module, which provides high-speed digital I/O between RTDS and external hardware.

In RSCAD FX, virtual CBs were placed on the MV and HV sides of the protected transformer (Group1Trans) to emulate real substation switching devices. Their operation was controlled by trip signals from the SEL IEDs. Specifically, outputs OUT101 and OUT102 from the SEL-487E commanded the MV and HV breakers, while OUT103 from the SEL-751A acted as a backup trip, operating only when the SEL-487E failed to clear a fault.

These digital outputs were linked to the CB control inputs via the GTFPI interface, enabling real-time breaker actuation and faulted-section isolation.

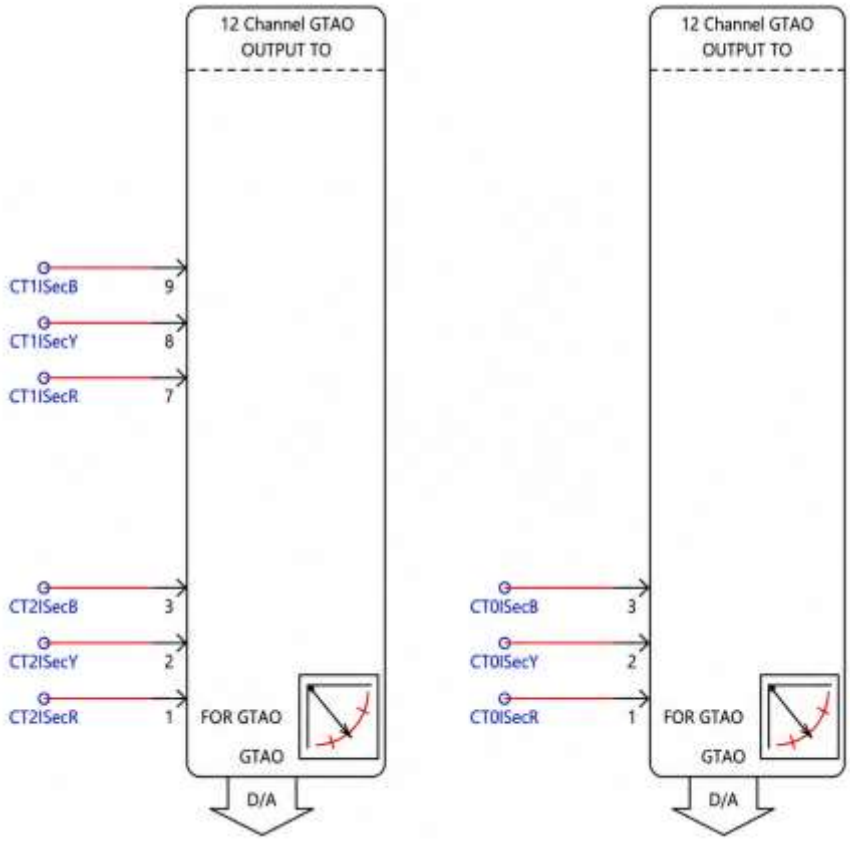


Fig. 2. GTAOs for the sampling of CT0, CT1, and CT2 signals. The input signals to the GTAO are connected from the secondary sides of the CTs

Fig. 3 illustrates the breaker control logic and its linkage to relay trip outputs, including latching logic, anti-bounce protection, and status feedback to emulate realistic CB operation. This closed-loop configuration was crucial for hardware-in-the-loop validation, ensuring that relay protection decisions based on simulated currents resulted in observable system-level actions within the RTDS environment. It also verified coordination between the primary relay, SEL-487E, and the backup relay, SEL-751A, with the SEL-487E successfully tripping and blocking the SEL-751A via GOOSE-based torque control. However, if the SEL-487E fails to act (due to simulated malfunction or deliberate suppression), the SEL-751A executes a delayed trip, providing redundant protection.

In summary, modeling the circuit breaker interface in RSCAD and integrating it with the SEL protection IEDs via GTFPI enabled a complete closed-loop simulation. This setup enabled real-time observation and verification of breaker actuation in response to protection logic decisions, ensuring a reliable, robust validation framework for the proposed IEC 61850-based protection scheme.

F. Configuration of IEC 61850 Communication

The implementation of the IEC 61850 standard was intended to facilitate high-speed, peer-to-peer communication between the SEL-487E and SEL-751A relays. This communication ensured the coordinated and selective operation of the protection scheme. Table VII summarizes the LNs configured on the SEL-487E relay. These LNs were linked to the 87R and 87U differential protection elements.

The LNs were incorporated into the configured IED description (CID) file, which served as the basis for defining datasets used in GOOSE messaging. Once a trip condition was detected by the SEL-487E, these datasets were transmitted to the SEL-751A through GOOSE communication to inhibit its operation when appropriate.

Table VIII summarizes the SEL-487E relay wordbits, IEC 61850 logical nodes, attributes, and corresponding protection functions used for GOOSE-based coordination with the SEL-751A relay.

This is an Open Access article distributed under the terms of the Creative Commons Attribution-Noncommercial 3.0 Unported License, permitting copy and redistribution of the material and adaptation for commercial and uncommercial use.

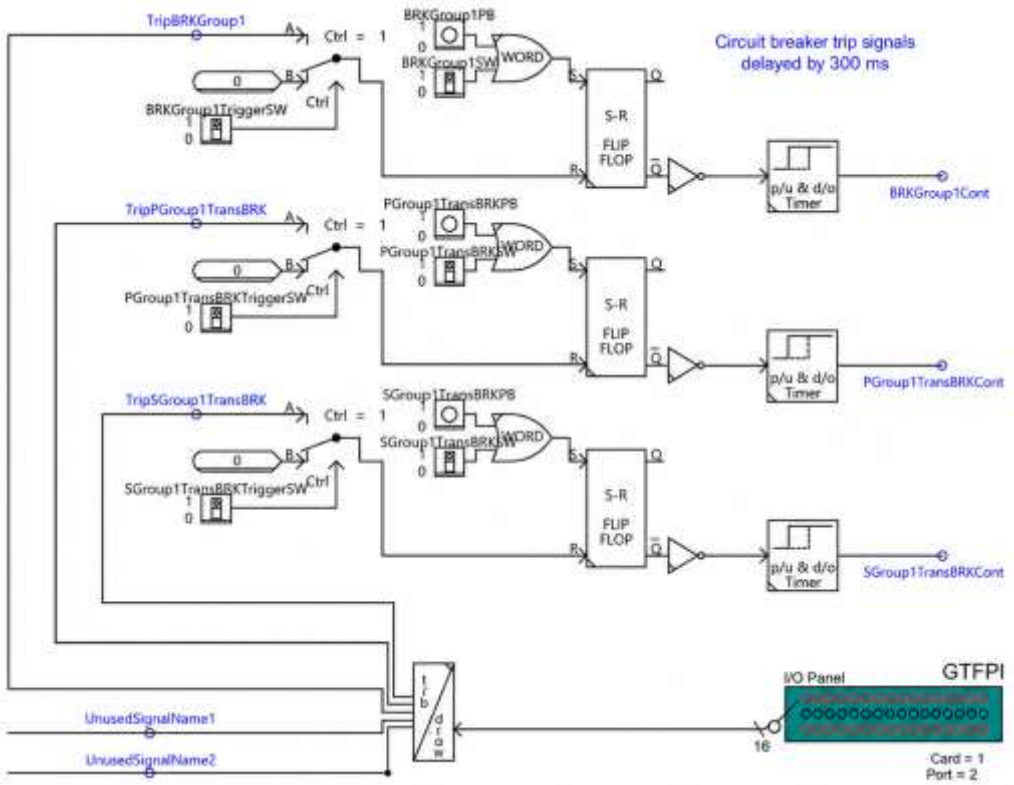


Fig. 3. Circuit breaker control logic through the GTFPI

Table VIII summarizes the SEL-487E relay wordbits, IEC 61850 logical nodes, attributes, and corresponding protection functions used for GOOSE-based coordination with the SEL-751A relay.

TABLE VIII
LIST OF SEL-487E RELAY WORDBITS AND PROTECTION LOGICAL

DATA SOURCE	LOGICAL NODE	ATTRIBUTE	COMMENT
87R[a]	D87RPDIF1	Op.general	Restrained differential element trip
87U[a]	D87UPDIF1	Op.general	Unrestrained differential element trip

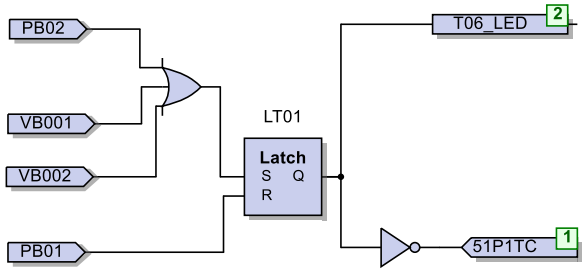


Fig. 4. Backup protection logic for blocking SEL-751A operation using GOOSE messages

Fig. 4 illustrates the backup protection logic for the SEL-487E and SEL-751A. The SEL-751A receives GOOSE messages via the virtual bits VB001 (87R) and VB002 (87U); activating either restrains tripping to prevent unnecessary breaker operation. If the SEL-487E fails to trip due to breaker or wiring faults, the SEL-751A operates after a preset delay to isolate the fault. Manual controls (PB01, PB02) manage latch and blocking functions, while the T06_LED indicator confirms receipt of a GOOSE message and active torque blocking.

In AcSELerator Architect, both the SEL-487E and SEL-751A IEDs were configured for GOOSE communication. Datasets were defined on the SEL-487E and mapped for transmission via virtual bits VB001 and VB002 to the SEL-751A, enabling proper data exchange. The resulting CID file was uploaded to each relay to complete the configuration.

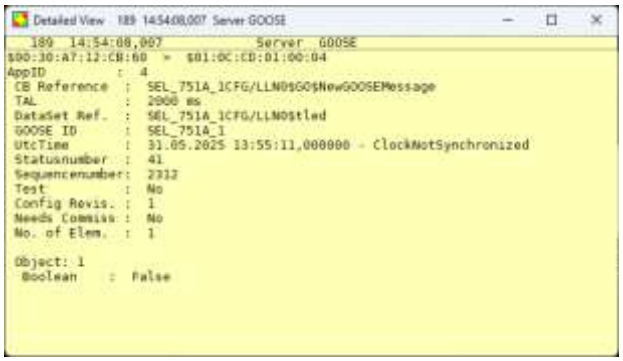


Fig. 5. GOOSE message status verification on SEL-751A

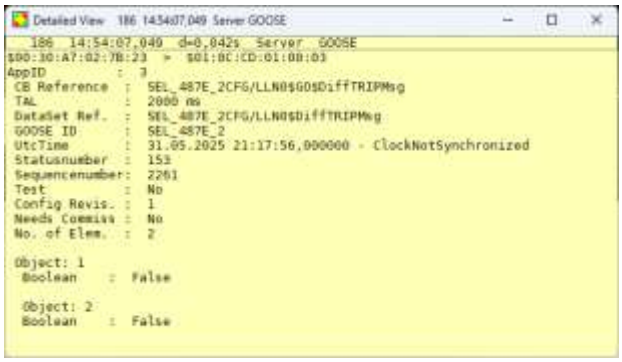


Fig. 6. GOOSE message server confirmation on SEL-487E

The GOOSE message server on the SEL-487E was validated using the demo version of GOOSE Inspector, confirming that communication links and dataset configurations between the two relays were correctly established and fully operational (Figs. 5–6). Although configuring the SEL-751A to transmit GOOSE messages was unnecessary, a minimal dataset was enabled to confirm successful publication. These configurations ensured reliable GOOSE message exchange, supporting deterministic coordination with a latency of 3–4 ms.

IV. Simulation and Testing of the Developed Protection Schemes

Two fault scenarios were simulated to assess the IEC 61850-based coordinated protection scheme. The first verified successful operation of the primary relay (SEL-487E), and the second simulated its trip failure, activating the backup relay (SEL-751A). These tests confirmed accurate fault detection, proper relay coordination, and reliable GOOSE communication under realistic smart-grid conditions, in accordance with established IEC 61850 coordination guidelines [5], [9], [11], [31].

A. Fault Scenario: Successful Operation of the SEL-487E Relay

Figs. A1–A2 in Appendix A show the event waveforms and binary signals for the successful SEL-487E trip. The differential current exceeded both restrained and unrestrained thresholds, prompting a trip within milliseconds. The RSCAD FX breaker opened upon receiving the signal, while GOOSE communication prevented unnecessary backup relay action. The internal fault was cleared in ~135 ms, consistent with IEC 61850 GOOSE latency benchmarks (<4 ms) [8], [9], [11], [35], confirming the reliability and speed of the primary differential protection.

B. Fault Scenario: Successful Operation of the SEL-487E Relay

Figs. B1–B3 in Appendix B show the event waveforms and binary signals for this condition. The SEL-487E correctly detected the internal fault, but the breaker failed to operate due to the simulated auxiliary malfunction. As a result, no GOOSE blocking signal (VB001/VB002) was sent to the SEL-751A, which initiated a delayed trip after its coordination interval. The fault was cleared by the SEL-751A after ~1.43 s, confirming expected fault detection, breaker failure, and backup relay operation. This behavior validates the coordination logic and supports the redundancy principles of differential overcurrent protection described in [5], [12].

C. Communication and Coordination Performance and Results Summary

Relay coordination and communication performance were assessed by monitoring the interaction between the SEL-487E and SEL-751A IEDs during testing. Differential and overcurrent thresholds were time-graded for selectivity, while GOOSE virtual bits (VB001 and VB002) provided torque blocking to prevent duplicate tripping, consistent with coordinated setting recommendations in [31], [32]. GOOSE messaging achieved consistent 3–4 ms transfer times, with successful publishing and subscribing between the relays, in agreement with previous IEC 61850 performance studies [11], [15].

Under identical transformer-zone fault conditions, the scheme cleared faults in 135 ms with the primary SEL-487E differential relay and in 1.43 s with the backup SEL-751A overcurrent relay. Conventional schemes without IEC 61850 coordination typically require 1.2–1.5 s [5], [6], [12]. The improvement resulted from eliminating hard-wired signaling delays, optimizing the 100 ms grading interval, and confirming deterministic coordination through HIL testing, aligning with prior communication-assisted protection studies [32], [34].

Overall, the IEC 61850-based coordinated framework demonstrated reliable performance under both normal and faulted conditions. Communication delays remained within acceptable real-time limits, and both relays operated selectively and dependably. HIL testing with RTDS/RSCAD FX and Omicron confirmed minimal delay and high-speed response, consistent with earlier validations [8], [34], [35].

Two scenarios were tested. In the first ("SEL-487E Trip Success"), the SEL-487E operated correctly, clearing the fault in 135 ms with no backup action. In the second ("SEL-487E Trip Failure – Breaker Fault"), the SEL-751A provided backup protection, clearing the fault in 1.43 s, reflecting the expected delay of secondary operation.

V. Conclusions, Recommendations, and Future Work

The study designed, implemented, and validated an IEC 61850-based multilayered protection scheme for high-voltage step-up transformers in a large-scale wind-farm-integrated smart grid. The results confirm that the framework operates effectively under both normal and faulted conditions, ensuring fast, reliable coordination between the primary and backup protection layers. The SEL-487E relay detected and isolated internal transformer faults within 135 ms, while the SEL-751A relay provided time-coordinated backup protection at approximately 1.43 s. IEC 61850 GOOSE-based communication achieved deterministic low-latency exchange with delays of 3–4 ms, consistent with benchmarks in [9], [15] and [35].

These findings are also consistent with recent studies emphasizing the continued importance of IEC 61850-based digital substations, GOOSE messaging, programmable digital twins, and low-latency communication for protection and automation in modern smart grids [17]–[21].

Hardware-in-the-loop validation using RTDS and Omicron current amplifiers confirmed the operational reliability of the proposed scheme under realistic conditions, aligning with practical IEC 61850 implementations reported in [32]. Coordination between the SEL-487E and SEL-751A relays eliminated hard-wired delays, improved IED interoperability, and achieved performance comparable to or exceeding that in [5], [8] and [12]. These results demonstrate the capability of IEC 61850-based communication to provide dependable, high-speed protection for critical transformer assets in networks integrating renewable energy. The relevance of this validation approach is further supported by recent HIL-based protection and monitoring studies, which show that real-time testing is essential for evaluating relay behavior, communication performance, and protection coordination before practical field deployment [22].

The main contribution lies in the experimental validation of a multilayered transformer protection scheme combining differential and overcurrent functions for wind-integrated smart grids. The study demonstrates practical GOOSE-based inter-relay coordination that enhances fault response speed and reliability, bridging the gap between simulation-only and real-time HIL implementations. The validation platform, based on a modified IEEE 9-bus system with an 18-unit wind farm model, establishes a scalable foundation for future testing and development. These outcomes align with smart-grid protection strategies that emphasize integrated, interoperable systems [32], [34]. They also respond to recent protection trends that call for adaptive, communication-assisted, and multilayer protection schemes capable of handling bidirectional power flow, converter-dominated fault behavior, and variable renewable-energy operating conditions [36], [38], [39], [43].

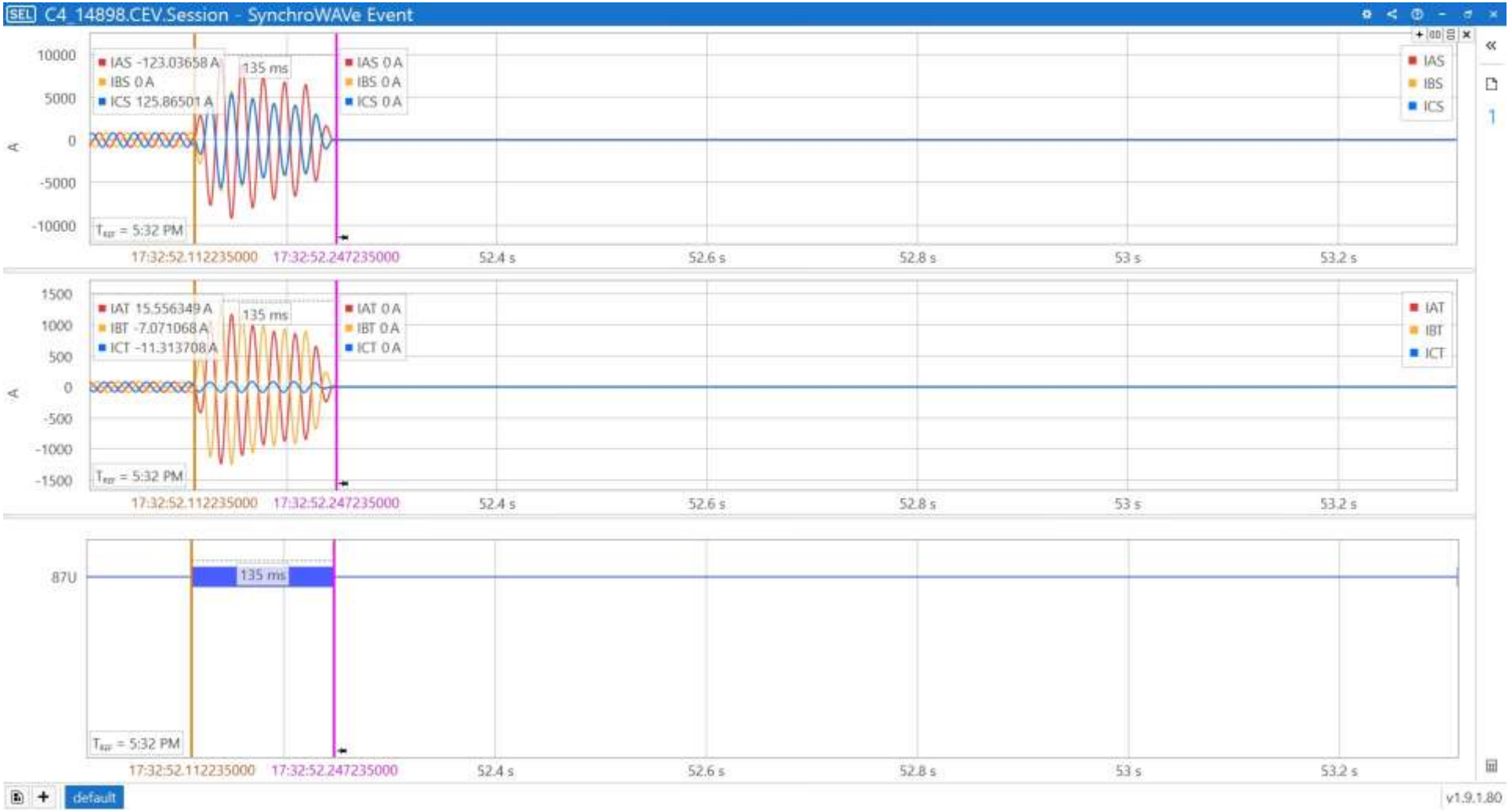
Certain limitations were noted. CTs were assumed to be linear and unsaturated, and only three-phase internal faults were analyzed. Fault types such as inter-turn and through faults, as well as IEC 61850-9-2 Sampled Values, were beyond scope. The test configuration included only SEL-487E, SEL-751A, and Omicron CMS devices, and cybersecurity mechanisms were not implemented, an essential consideration for future digital protection research. Furthermore, recent studies on inverter-based resource protection indicate that converter-interfaced renewable generation can significantly affect fault-current magnitude, direction, and frequency, which may influence the performance of differential, distance, and overcurrent protection under more diverse operating conditions [23]–[26]. These issues should therefore be considered in future extensions of the proposed protection framework.

Future work should include inter-turn and through-fault tests, magnetizing inrush conditions, and integration of IEC 61850-9-2 SVs and IEC 61850-90-5 for enhanced interoperability. Implementing encryption and authentication, as suggested in [35], would further strengthen cyber resilience. Field validation in operational substations is also recommended to confirm robustness under real-world conditions. These directions align with current trends toward adaptive, interoperable, and cyber-secure smart-grid protection [16], [33], [34].

Additional future work should also investigate active-power-based, data-driven, and high-frequency-impedance-based protection methods, as recent studies have shown their potential to improve sensitivity, selectivity, and dependability in renewable-energy-integrated and wind-farm transmission systems [27]–[30].

Overall, the study concludes that IEC 61850-based coordinated protection schemes validated through HIL testing offer a reliable, fast, and future-ready solution for high-voltage transformer protection in renewable energy networks.

Appendix A



This is an Open Access article distributed under the terms of the Creative Commons Attribution-Noncommercial 3.0 Unported License, permitting copy and redistribution of the material and adaptation for commercial and uncommercial use.

Fig. A1. Event report waveforms and binary signals extracted from the SEL-487E relay when it successfully issued a trip signal to the circuit breaker for an internal fault

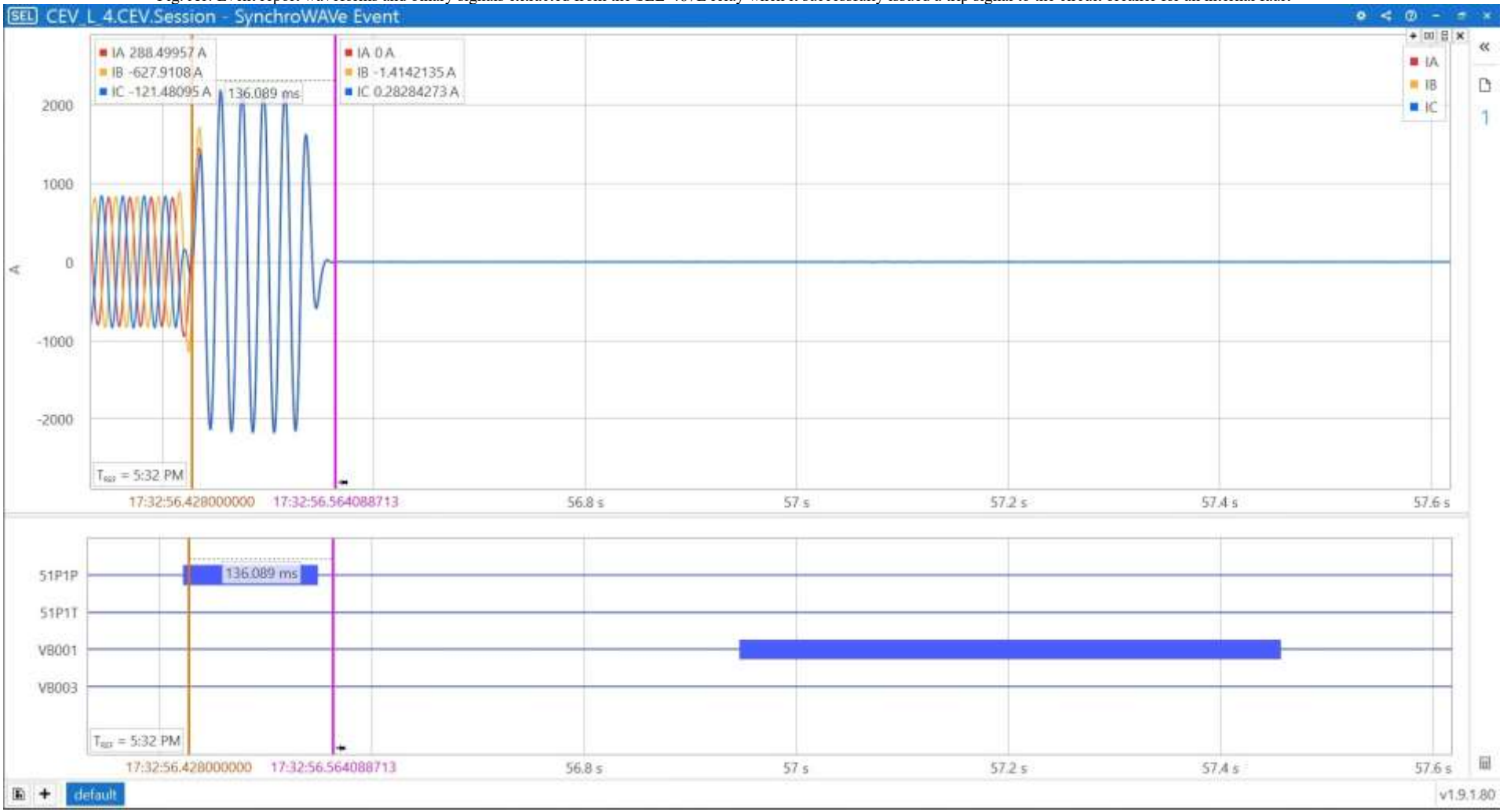


Fig. A2. Event report waveforms and binary signals extracted from the SEL-751A relay when the SEL-487E relay successfully issued a trip signal to the circuit breaker for an internal fault

Appendix B

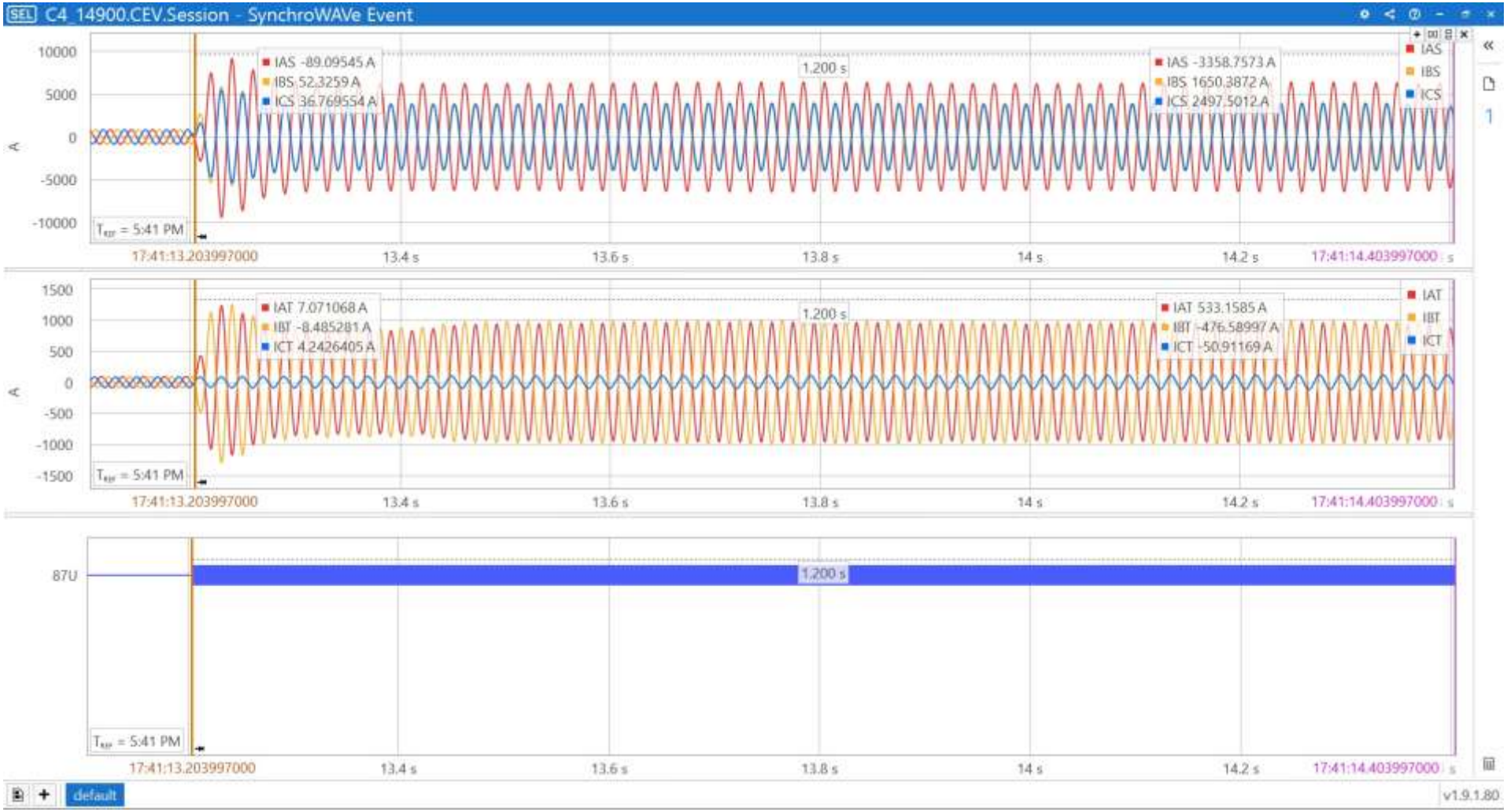


Fig. B1. Event report waveforms and binary signals extracted from the SEL-487E relay when it failed to issue a trip signal to the circuit breaker for an internal fault

This is an Open Access article distributed under the terms of the Creative Commons Attribution-Noncommercial 3.0 Unported License, permitting copy and redistribution of the material and adaptation for commercial and uncommercial use.

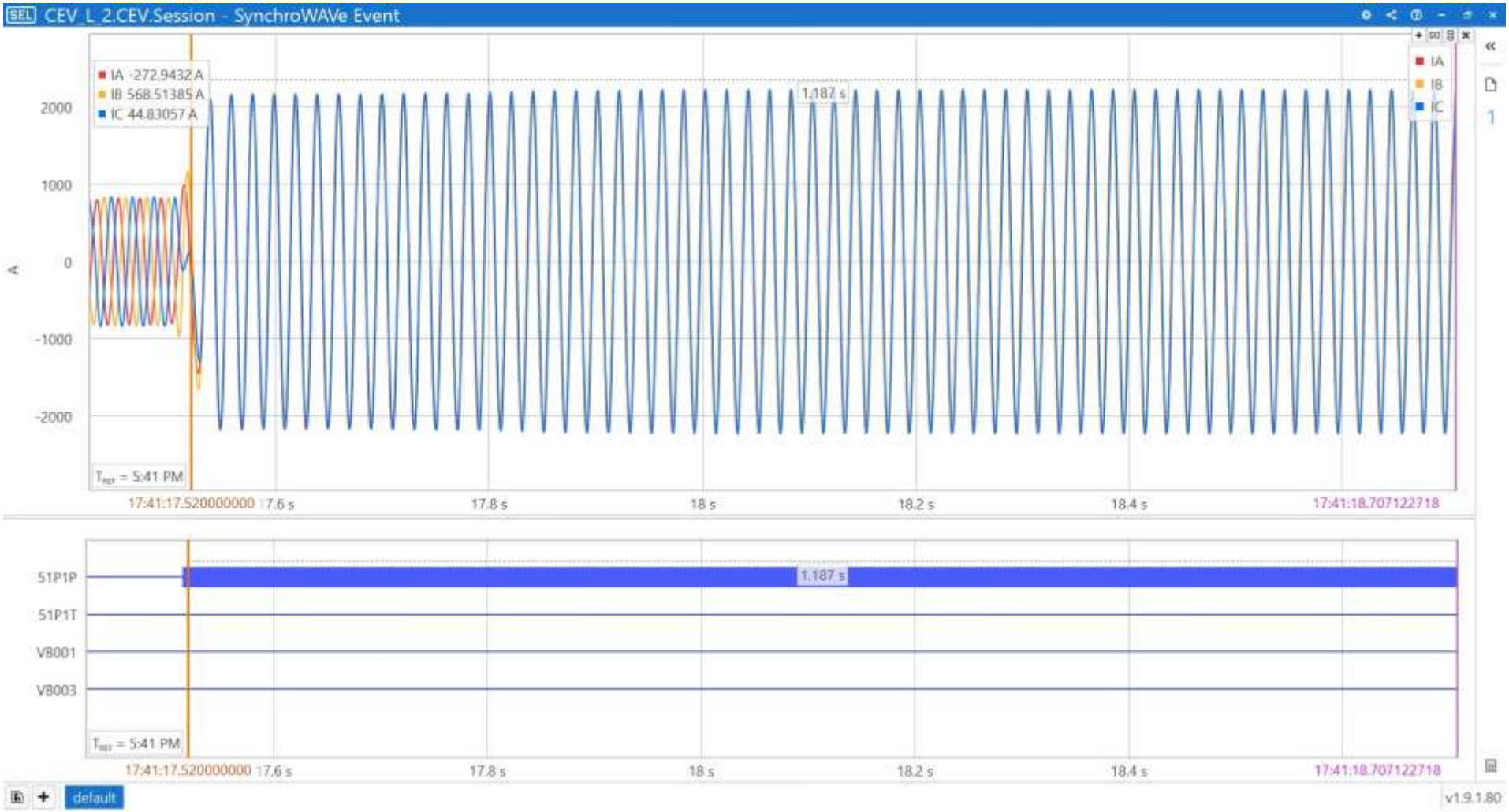


Fig. B2. Path a). Event report waveforms and binary signals extracted from the SEL-751A relay when the SEL-487E failed to issue a trip signal to the circuit breaker for an internal fault

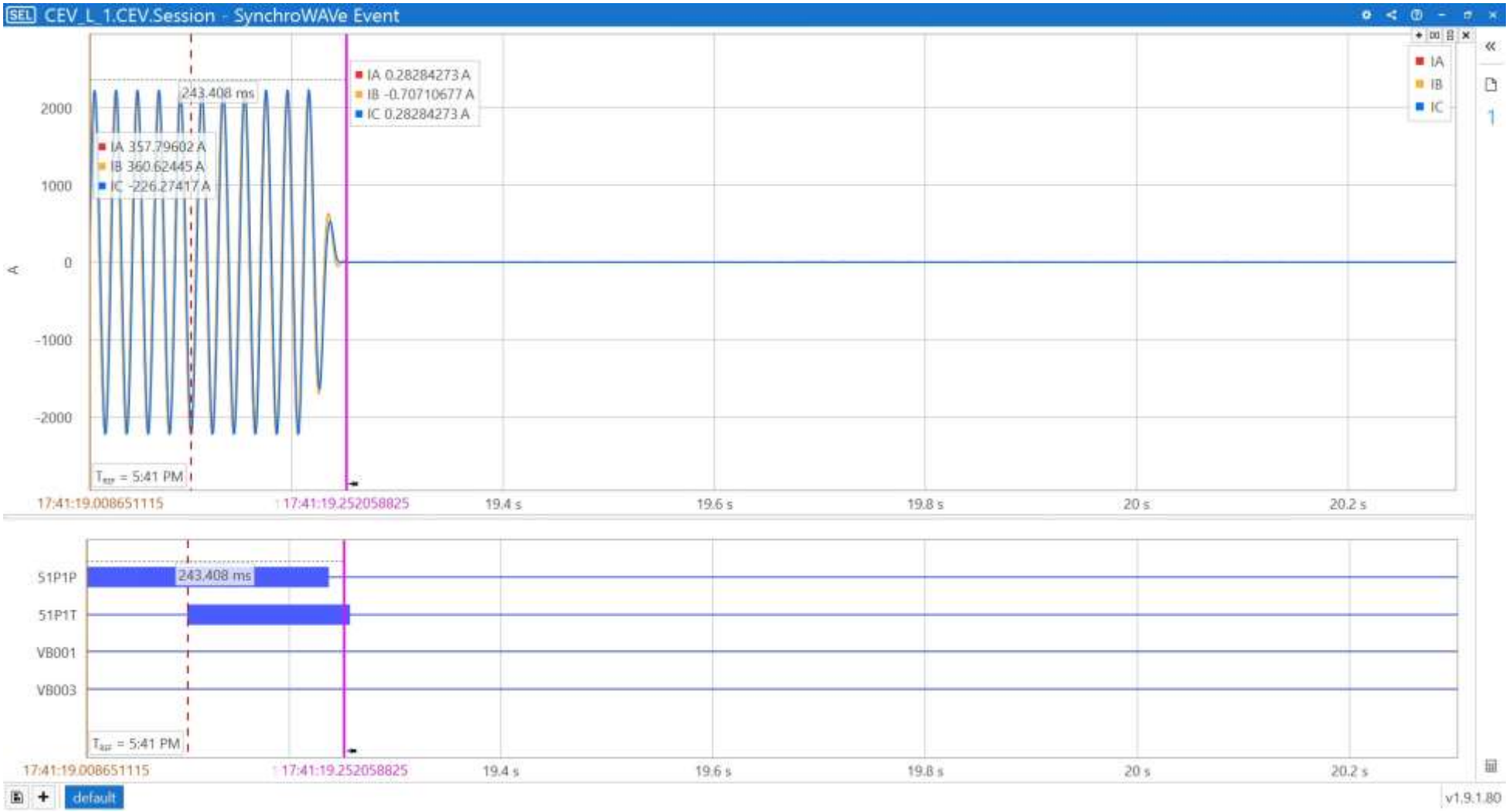


Fig. B3. Path b). Event report waveforms and binary signals extracted from the SEL-751A relay when the SEL-487E failed to issue a trip signal to the circuit breaker for an internal fault

Conflict of Interest

The authors declare no conflict of interest in the publication process of the research article.

Author Contributions

Y. Gcelu: Conceptualization of the coordinated protection scheme; modeling and implementation of the modified IEEE 9-bus and large-scale wind-farm system in RTDS/RSCAD FX; development and configuration of the SEL-487E primary differential protection scheme; execution of HIL experiments; data acquisition and analysis; and preparation of the original manuscript draft.

M. E. S. Mnguni: Supervision of system modeling, protection-scheme design, and RTDS integration; technical validation of the differential and overcurrent protection logic; critical review and editing of the manuscript; guidance on the interpretation of HIL results; and oversight of the research methodology.

S. Nomandela: Co-supervision and technical guidance on the simulation conceptualization, smart-grid modeling approach, and large-scale wind-farm integration in RTDS/RSCAD FX; contribution to simulation-related design decisions and validation strategy; technical consultancy on the IEC 61850 communication architecture; configuration and verification of GOOSE-based coordination; analysis of communication latency and relay-coordination performance; manuscript review and refinement; and project administration support.

References

[1] A. S. Anees, "Grid Integration of Renewable Energy Sources: Challenges, Issues and Possible Solutions," in *2012 IEEE 5th India International Conference on Power Electronics (IICPE)*, Dec. 2012, pp. 1–6. doi: 10.1109/IICPE.2012.6450514.

[2] X. Song, Z. Meng, K. Chang, F. Xue, and L. Zhou, "Dynamic Reactive Power Compensation during Fault Conditions for Wind Farms with the Consideration of Wind Turbine Protection Effects," in *IET Conference Publications*, 2012, p. 120. doi: 10.1049/cp.2012.1819.

[3] A. Han, Z. Zhang, and X. Yin, "The impacts of distributed doubly-fed induction generators on smart distribution Grid protection," *Model. Identif. Control (ICMIC), 2010 Int. Conf.*, pp. 71–75, 2010.

[4] H. Ibrahim, M. Ghandour, M. Dimitrova, A. Ilinca, and J. Perron, "Integration of Wind Energy into Electricity Systems: Technical Challenges and Actual Solutions," *Energy Procedia*, vol. 6, pp. 815–824, 2011, doi: 10.1016/j.egypro.2011.05.092.

[5] S. P. George and S. Ashok, "Modified Differential Protection for Transformers in Wind Farms," *J Electr Eng Technol*, no. 9, pp. 78–88, 2018, doi: http://doi.org/10.5370/JEET.2018.13.1.078.

[6] B. Gao, W. Wei, L. Zhang, N. Chen, Y. Wu, and Y. Tang, "Differential Protection for an Outgoing Transformer of Large-scale Doubly Fed Induction Generator-based Wind Farms," *Energies*, vol. 7, no. 9, pp. 5566–5585, 2014, doi: 10.3390/en7095566.

[7] M. A. Ahmed *et al.*, "Communication Network Architectures for Southwest Offshore Wind Farm," *IET Conf. Publ.*, vol. 7, no. 4, pp. 1–6, 2014, doi: 10.1049/cp.2011.0101.

[8] J. Cardenas, V. Muthukrishnan, D. McGinn, and R. Hunt, "Wind Farm Protection Using an IEC 61850 Process Bus Architecture," in *10th IET International Conference on Developments in Power System Protection (DPSP 2010), Managing the Change, Manchester, UK, 29 March–1 April 2010*, 2010, pp. 1–5.

[9] S. M. Saad, A. Elhaffar, and K. El-arroudi, "Optimizing Differential Protection Settings for Power Transformers," in *2015 Modern Electric Power Systems (MEPS)*, IEEE, 2015, pp. 1–6. doi: 10.1109/MEPS.2015.7477186.

[10] R. P. Medeiros, F. B. Costa, and K. M. Silva, "Power Transformer Differential Protection Using the Boundary Discrete Wavelet Transform," *IEEE Trans. Power Deliv.*, vol. 31, no. 5, pp. 2083–2095, 2016, doi: 10.1109/TPWRD.2015.2513778.

[11] B. E. M. Camachi, O. Chenaru, L. Ichim, and D. Popescu, "A Practical Approach to IEC 61850 Standard for Automation, Protection and Control of Substations," in *Proceedings of the 9th International Conference on Electronics, Computers and Artificial Intelligence, ECAI 2017*, 2017, pp. 1–6. doi: 10.1109/ECAI.2017.8166471.

[12] J. Ma, W. Zhang, J. Liu, and J. S. Thorp, "A novel adaptive distance protection scheme for DFIG wind farm collector lines," *Int. J. Electr. Power Energy Syst.*, vol. 94, pp. 234–244, 2018, doi: 10.1016/j.ijepes.2017.07.008.

[13] T. Y. Zheng, S. T. Cha, P. A. Crossley, and Y. C. Kang, "Protection algorithm for a wind turbine generator based on positive- and negative-sequence fault components," *APAP 2011 - Proc. 2011 Int. Conf. Adv. Power Syst. Autom. Prot.*, vol. 2, pp. 1115–1120, 2011, doi: 10.1109/APAP.2011.6180548.

[14] R. Cai and B. Su, "Study on protection of large scale wind power integration," *APAP 2011 - Proc. 2011 Int. Conf. Adv. Power Syst. Autom. Prot.*, vol. 3, pp. 1718–1722, 2011, doi: 10.1109/APAP.2011.6180760.

[15] M. A. Ahmed and Y.-C. Kim, "Communication Network Architectures for Southwest Offshore Wind Farm," *J. Korean Inst. Commun. Inf. Sci.*, vol. 42, no. 1, pp. 88–97, 2017, doi: 10.7840/kics.2017.42.1.88.

[16] B. Li, Y. Sheng, J. He, Y. Li, Z. Xie, and Y. Cao, "Improved Distance Protection for Wind Farm Transmission Line Based on Dynamic Frequency Estimation," *Int. J. Electr. Power Energy Syst.*, vol. 153, no. July, 2023, doi: 10.1016/j.ijepes.2023.109382.

[17] H. Lopez, E. Pashajavid, S. Rajakaruna, Y. Liu, and Y. Yin, "Development of Programmable Digital Twin via IEC-61850 Communication for Smart Grid," *Energies*, vol. 19, no. 3, pp. 1–15, 2026, doi: 10.3390/en19030703.

[18] A. Kniphoff da Cruz, A. C. Hackenhaar Kellermann, I. C. da Silva, J. M. Fernandes de Oliveira, M. E. Jochims Kniphoff da Cruz, and L. Däubler, "IEC 61850 GOOSE: A Systematic Literature Review on the State of the Art and Current Applications," *Automation*, vol. 7, no. 2, pp. 1–42, 2026, doi: 10.3390/automation7020062.

[19] D. B. Tastan and M. Balta, "Anomaly Detection for Substations Based on IEC 61850-NFA Model," *Appl. Sci.*, vol. 16, no. 8, pp. 1–31, 2026, doi: 10.3390/app16084000.

[20] A. Kniphoff da Cruz, C. Siemers, L. Däubler, and A. C. Hackenhaar Kellermann, "Integration Method for IEC 61850 into Legacy and Modern PLC Systems," *Automation*, vol. 7, no. 1, p. 7, 2026, doi: 10.3390/automation7010007.

[21] H. Z. Kazme, P. Westerlund, and M. H. J. Bollen, "Evaluating 5G Communication for IEC 61850 Digital Substations: Historical Context and Latency Challenges," *Energies*, vol. 18, no. 16, 2025, doi: 10.3390/en18164387.

[22] S. Nomandela, M. E. S. Mnguni, and A. K. Raji, "Systematic Development and Hardware-in-the-Loop Testing of an IEC 61850 Standard-Based Monitoring and Protection System for a Modern Power Grid Point of Common Coupling," *Energies*, vol. 18, no. 19, pp. 1–47, 2025, doi: 10.3390/en18195281.

[23] Z. Su, Q. Chen, S. Wang, Z. Qin, and J. Gao, "Differential Protection Based on Virtual Short-Circuit Current Considering Both Grid-Forming Inverter and Grid-Following Inverter for New Energy Bases," *Energies*, vol. 19, no. 8, 2026, doi: 10.3390/en19081853.

[24] G. Sarode, M. Bhatkar, and S. Paladhi, "Distance Protection for

This is an Open Access article distributed under the terms of the Creative Commons Attribution-Noncommercial 3.0 Unported License, permitting copy and redistribution of the material and adaptation for commercial and uncommercial use.

Power Grids with Inverter-Based Resources : Challenges , Probable Solutions and Future Research Opportunities," *Electricity*, vol. 7, pp. 1–36, 2026.

[25] W. Zhou, Z. Zhou, X. Li, W. Chen, H. Wang, and B. Luo, "Adaptive Sampled Value Differential Protection With High Penetration of Inverter-Based Resource Based on Error Function Fitting," *IEEE Access*, vol. 13, no. July, pp. 136473–136482, 2025, doi: 10.1109/ACCESS.2025.3592952.

[26] R. Pujari and M. Nabab Alam, "Distance Relaying for the Protection of Modern Power System Networks," *IEEE Access*, vol. 13, no. February, pp. 28861–28893, 2025, doi: 10.1109/ACCESS.2025.3539919.

[27] Y. Xie, C. Wu, M. Cheng, D. Zhang, X. Zhang, and Q. Chen, "Active Power Criterion Based High-Adaptive Differential Protection for Power Electronic Equipment," *Energies*, vol. 19, pp. 1–15, 2026.

[28] H. Shi *et al.*, "Smart Protection Relay for Power Transformers Using Time-Domain Feature Recognition," *Processes*, vol. 14, no. 3, pp. 1–22, 2026, doi: 10.3390/pr14030449.

[29] C. Kishore, M. Tripathy, R. Nandi, L. Xu, and A. Egea-Alvarez, "A Novel Differential Fault Detection Strategy for Smart AC Microgrid Incorporating Tapped Loads," *IEEE Trans. Ind. Informatics*, vol. 21, no. 12, pp. 9678–9689, 2025, doi: 10.1109/TII.2025.3606199.

[30] C. Yang, Y. Tang, J. Wang, J. Zhou, and Y. Pu, "A Pilot Differential Protection Scheme Based on Dominant Frequency Band for the Outgoing Lines of Inverter-Interfaced Renewable Energy Generator Station," *IEEE Access*, vol. 12, no. December, pp. 190922–190935, 2024, doi: 10.1109/ACCESS.2024.3517753.

[31] T. S. Ustun, C. Ozansoy, and A. Zayegh, "Simulation of Communication Infrastructure of a Centralized Microgrid Protection System Based on IEC 61850-7-420," *2012 IEEE Third Int. Conf. Smart Grid Commun.*, pp. 492–497, 2012, doi: 10.1109/SmartGridComm.2012.6486033.

[32] P. H. A. Barra, V. A. Lacerda, R. A. S. Fernandes, and D. V Coury, "A Hardware-In-the-Loop Testbed for Microgrid Protection Considering Non-standard Curves ☆," *Electr. Power Syst. Res.*, vol. 196, no. November 2020, p. 107242, 2021, doi: 10.1016/j.epsr.2021.107242.

[33] M. B. Member *et al.*, "Real Time Simulation of Smart Grids for Interface Protection Test and Analysis," *Proc. 14th Int. Conf. Harmon. Qual. Power - ICHQP 2010*, pp. 1–6, 2010, doi: 10.1109/ICHQP.2010.5625444.

[34] F. Alasali *et al.*, "The Recent Development of Protection Coordination Schemes based on Inverse of AC Microgrid : A Review," no. November 2023, pp. 1–23, 2024, doi: 10.1049/gtd2.13074.

[35] S. M. Alizadeh and C. Ozansoy, "The Role of Communications and Standardization in Wind Power Applications - A Review," *Renew. Sustain. Energy Rev.*, vol. 54, pp. 944–958, 2016, doi: 10.1016/j.rser.2015.10.061.

[36] L. F. Serna-Montoya, S. D. Saldarriaga-Zuluaga, J. M. López-Lezama, and N. Muñoz-Galeano, "Optimal Microgrid Protection Coordination for Directional Overcurrent Relays Through Mixed-Integer Linear Optimization," *Energies*, vol. 18, no. 8, pp. 1–31, 2025, doi: 10.3390/en18082035.

[37] K. Islam, D. Kim, and A. Abu-siada, "A Review on Adaptive Power System Protection Schemes for Future Smart and Micro Grids, Challenges and Opportunities," *Electr. Power Syst. Res.*, vol. 230, no. February, p. 110241, 2024, doi: 10.1016/j.epsr.2024.110241.

[38] S. Shazdeh, H. Golpîra, and H. Bevrani, "Advanced and Smart Protection Schemes in Renewable Integrated Power Systems: A survey and New Perspectives," *Electr. Power Syst. Res.*, vol. 235, no. June, 2024, doi: 10.1016/j.epsr.2024.110832.

[39] M. A. Ajith and R. M. Shereef, "Islanding and Fault Detection of Inverter Based Distributed Generations Using Wavelet Packet Transform and Ensemble," *Electr. Power Syst. Res.*, vol. 231, no. April, p. 110356, 2024, doi: 10.1016/j.epsr.2024.110356.

[40] S. Nomandela, M. E. S. Mnguni, and A. K. Raji, "A Case Study on the Validation of Renewable Energy Grid Code Compliance for a Large-Scale Wind Power Plant Grid-Connected Mode of Operation in Real-Time Simulation," *Appl. Sci.*, vol. 15, no. 5521, pp. 1–38, 2025, doi: 10.3390/app15105521.

[41] B. M. Weedy, B. J. Cory, N. Jenkins, J. B. Ekanayake, and G. Strback, *Electric Power Systems*, Fifth Edit. Hoboken, NJ, USA: Wiley, 2012.

[42] IEEE, *IEEE Guide for the Application of Current Transformers Used for Protective Relaying Purposes - Redline*, vol. 2007, no. April. 2008.

[43] K. Islam, D. Kim, and A. Abu-Siada, "A Review on Adaptive Power System Protection Schemes for Future Smart and Micro Grids, Challenges and Opportunities," *Electr. Power Syst. Res.*, vol. 230, no. February, p. 110241, 2024, doi: 10.1016/j.epsr.2024.110241.